Research Article

Hongzhao Qi*, Jie Yang, Jie Yu, Lijun Yang, Peipei Shan, Sujie Zhu, Yin Wang, Peifeng Li, Kun Wang, and Qihui Zhou*

Glucose-responsive nanogels efficiently maintain the stability and activity of therapeutic enzymes

https://doi.org/10.1515/ntrev-2022-0095
received January 29, 2022; accepted March 17, 2022

Abstract: To date, the encapsulation of therapeutic enzymes in a protective matrix is an optimized strategy for the maintenance of their stability, facilitating their clinical application. However, the stability and activity of therapeutic enzymes are often in tension with each other. A rigid protective matrix may effectively maintain the stability of therapeutic enzymes, but it can reduce the diffusion of substrates toward the therapeutic enzyme active site, dramatically affecting their catalytic efficiency. Here, we exploited a kind of nanogels by *in situ* polymerization on the arginine deiminase (ADI) surface with 3-acrylamidophenylboronic acid (APBA) monomer. These nanogels efficiently improved the thermal stability (25–75°C), the pH stability (pH 1–13), and protease (trypsin) stability of ADI due to the strong rigidity of the surface poly(APBA) shell. And even after 60 days of storage, ~60% of the activity of ADI encapsulated by nanogels remained. Furthermore, ADI encapsulated by nanogels could efficiently degrade arginine to increase the ratio of citrulline to arginine in mice plasma. That is because autologous glucose binds with APBA leading to the hydrophilicity increase of nanogels, and then, the arginine molecules can readily diffuse toward the encapsulated ADI. This nanogel platform eases the tension between the stability and activity of therapeutic enzymes. The resulting nanogels can efficiently maintain the *in vitro* stability and the *in vivo* activity of therapeutic enzymes, facilitating the exploitation of new therapeutic enzyme formulations, which can be transported and stored *in vitro* for a long time and be applied effectively *in vivo*.

Keywords: therapeutic enzyme, activity, stability, nanogel, hydrophobicity, hydrophilicity

1 Introduction

Therapeutic enzymes have been applied to clinical practice for at least 60 years [1]. As an example, De Duve [2] has first reported that a therapeutic enzyme can be a part of replacement therapies for genetic deficiencies. To date, they have been used to treat various diseases, such as COVID-19 and cancers [3–6]. Compared with other kinds of drugs, such as nucleic acid drugs [7], therapeutic enzymes can specially bind and efficiently act on target molecules. Furthermore, the target molecules of therapeutic enzymes are often multiple, endowing them with a broad spectrum of therapeutic ability [8]. Therapeutic enzymes have been used to treat various disorders that small molecules cannot treat. As an example, arginine deiminase (ADI) is a kind of therapeutic enzyme used for arginine (Arg) deprivation that can efficiently suppress argininosuccinate synthetase (ASS1)-deficient tumors. Under normal circumstances, Arg is a kind of nonessential amino acid since normal cells can convert citrulline (Cit) to Arg *via* the catalysis of ASS1, while ASS1-deficient tumor cells must rely on exogenous Arg to meet the needs of growth and proliferation. Therefore, ASS1-deficient tumors can be efficiently suppressed by ADI-based degradation of the Arg in the blood. However, therapeutic enzymes are proteins with complex and fragile three-dimensional structures, which are easily destroyed by

* **Corresponding author: Hongzhao Qi,** Institute of Translational Medicine, The Affiliated Hospital of Qingdao University, College of Medicine, Qingdao University, Qingdao 266021, China, e-mail: qihongzhao@qdu.edu.cn
* **Corresponding author: Qihui Zhou,** Institute of Translational Medicine, The Affiliated Hospital of Qingdao University, College of Medicine, Qingdao University, Qingdao 266021, China, e-mail: qihuizhou@qdu.edu.cn
Jie Yang: Department of Traditional Chinese Medicine, Liaocheng Dongchangfu People's Hospital, Liaocheng 252003, China
Jie Yu: Qingdao Center Hospital, Qingdao Center Medical Group, Qingdao 266042, China
Lijun Yang: Qingdao Institute of Bioenergy and Bioprocess Technology, Chinese Academy of Sciences, Qingdao 266101, China
Peipei Shan, Sujie Zhu, Yin Wang, Peifeng Li, Kun Wang: Institute of Translational Medicine, The Affiliated Hospital of Qingdao University, College of Medicine, Qingdao University, Qingdao 266021, China

high temperature, pH, organic solvents, or proteases [9–11]. The low stability of therapeutic enzymes would limit their *in vitro* transportation and storage and reduce their *in vivo* catalytic efficiency [12,13]. The enhancement of therapeutic enzyme stability, therefore, is extremely necessary to realize their efficient clinical application.

To improve the stability of therapeutic enzymes under harsh conditions, numerous strategies have been applied. Thereinto, the conjugation of polyethylene glycol (PEG) to therapeutic enzymes (PEGylation) is one of the most successful strategies to maintain their stability [14]. However, the reduced bioactivity of therapeutic enzymes caused by the random chemical coupling greatly limited their practical application [15]. Besides, immobilization of therapeutic enzymes on scaffolds, which can achieve stabilization effects to maintain the three-dimensional structure of therapeutic enzymes, is used to improve their stability [16]. However, therapeutic enzymes immobilized on macroscaffolds can only be used locally, limiting their application scope [17]. Microscaffolds, such as organic/inorganic nanoparticles, can be applied for the immobilization of therapeutic enzymes realizing their systemic and local application, but the structural stability and catalytic activity of therapeutic enzymes are strongly affected by the physicochemical properties of biointerfaces, such as porosity, surface curvature, and their heterogeneity [18–22]. Immobilization of therapeutic enzymes often results in the lower catalytic activity because the structure of the therapeutic enzyme is easily destroyed [22]. Encapsulation of therapeutic enzymes in a protective matrix, by comparison, is an optimized method to maintain their stability. For example, Zhang *et al.* have reported a therapeutic enzyme encapsulation technology that is based on a zwitterionic polymer network, efficiently enhancing their stability, improving their pharmacokinetics, and mitigating the immune response [23]. Taking advantage of the rigidity of the protective matrix to maintain the three-dimensional conformation of therapeutic enzymes is the fundamental mechanism of encapsulation methods [24]. Theoretically, the more rigid the protective matrix is, the stronger the stability of therapeutic enzymes is. However, their activity and stability are commonly in tension with each other. A rigid matrix layer surrounding the therapeutic enzymes may effectively maintain their structure, but it can reduce the diffusion of substrates, dramatically affecting their catalytic efficiency [25,26]. Therefore, how to address the tension between the stability and activity of therapeutic enzymes is a huge challenge for therapeutic enzyme encapsulation technologies.

As shown in Scheme 1, we used ADI as a model therapeutic enzyme, and the *in situ* polymerization on ADI surface with 3-acrylamido-phenylboronic acid (APBA), *N*-(3-aminopropyl)methacrylamide (APM), and *N*,*N*′-methylene-bis(acrylamide) (BIS) was adopted to exploit a kind of nanogel (denoted as P-n(ADI)). To further endow P-n(ADI) with the high *in vivo* application capacity, it was combined with PEG to form PEGylated P-n(ADI) (denoted as PP-n(ADI)). These nanogels showed strong rigidity *in vitro* because of the hydrophobicity of poly(APBA) [27]. The rigid polymeric shell could efficiently restrain conformational changes in ADI, dramatically maintaining the *in vitro* stability of ADI. Once inside the body, APBA molecules located at the surface of PP-n(ADI) could bind with autologous glucose increasing the hydrophilicity and flexibility of the poly(APBA) shell [28]. PP-n(ADI) bound with glucose was denoted as PP-n(ADI)/Glucose. The concentration of glucose was 5 mM similar to the physiological level of glucose unless otherwise mentioned. Then, the Arg molecules could readily diffuse toward the encapsulated ADI, efficiently maintaining the catalytic activity of ADI. Furthermore, the flexible poly(APBA) shell can still protect ADI from degradation and improve its *in vivo* stability. This kind of nanogel could facilitate the exploitation of new therapeutic enzyme formulations, which can be transported and stored *in vitro* for a long time and be applied effectively *in vivo*.

2 Experimental section

2.1 Materials

Rough extracted ADI was purchased from Baiaolaibo Technology Co., Ltd (Beijing, China). Methoxy PEG propionaldehyde (mPEG-ALD, MW 5 kDa) was provided by Jenkem Technology Co., Ltd (Beijing, China). Bicinchoninic acid (BCA) protein assay kit, Sephadex G-100, and Cell Counting Kit-8 (CCK-8) were supplied by Solarbio (Beijing, China). Amino acid assay kits were bought from BioVision Incorporated. Fluorescein isothiocyanate (FITC) isomer was purchased from Yuanye Biological Technology Co., Ltd (Shanghai, China). Annexin V-FITC/PI cell apoptosis assay kit was bought from Meilunbio Co., Ltd (Dalian, China). Other unindicated chemical reagents were purchased from Sigma.

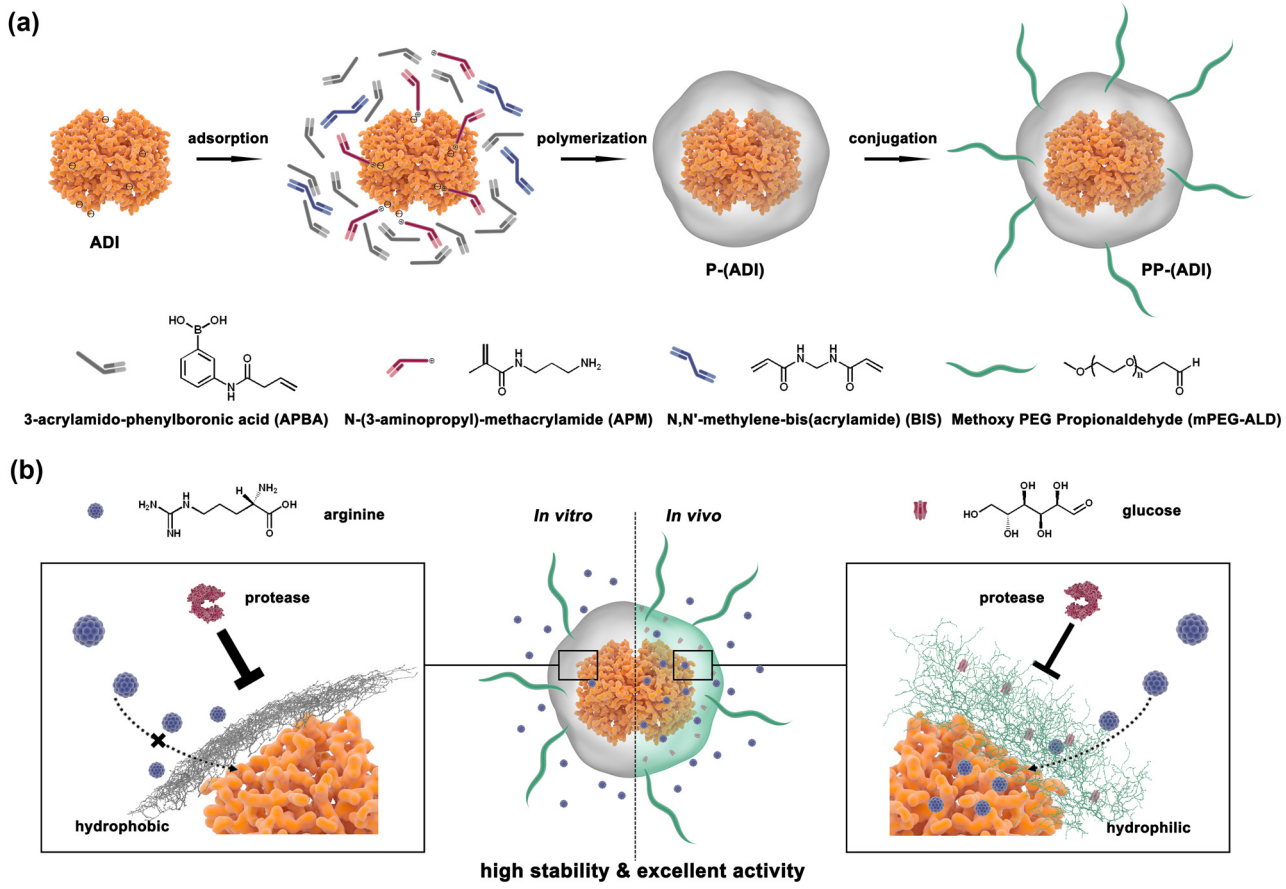

Scheme 1: The mechanism for the preparation and action of nanogels. (a) APBA, APM, and BIS were added to ADI solution and they could enrich around ADI molecules because of the hydrogen bond and hydrophobic interaction between them. Then, P-n(ADI) was formed by initiating the free radical polymerization of monomers and crosslinkers. mPEG-ALD was linked to P-n(ADI) to form PP-n(ADI). (b) The polymeric shell was hydrophobic *in vitro*, efficiently maintaining the stability of ADI. Glucose bound with APBA molecules can locate at the polymeric shell leading to the loosening of nanogels and the restoration of the catalytic activity of ADI. In addition, the loosened polymeric shell still had protective effects.

2.2 The PP-n(ADI) synthesis and its characteristics

PP-n(ADI) was synthesized according to the previous method with slight modification [29]. Crude enzyme extract was filtered by Sephadex G-100 to obtain pure ADI, which was further quantified by a BCA assay kit. To facilitate the encapsulation, ADI (10 mg/mL) was first mixed with *N*-hydroxysuccinimide ester (the molar ratio was 1:20) at 4°C for 24 h, and the acrylated ADI was purified by dialyzing against phosphate-buffered saline (PBS). The acrylated ADI (1 mg/mL) was mixed with APM, APBA, and BIS (the molar ratio was 1:300:3,000:300). The polymerization was initiated by taking advantage of ammonium persulfate as the initiator and *N*,*N*,*N*′,*N*′-tetramethylethylenediamine as the catalyst, and it was carried out under the protection of nitrogen at 4°C for 2 h. The resulting P-n(ADI) was purified by dialyzing against PBS and using a hydrophobic interaction column (Phenyl-Sepharose CL-4B). The ADI loading capacity was determined by a BCA assay kit. To further prepare PP-n(ADI), mPEG-ALD was mixed with P-n(ADI) in the alkaline buffer overnight. The molar ratio of mPEG-ALD to P-n(ADI) (by ADI mass) was 20. The uncoupled PEG was removed by dialyzing against PBS. Bovine serum albumin (BSA) could be used as an ADI substitute, and PP-n(BSA) could be prepared as the above-mentioned method.

The size distribution and zeta potential of samples were measured by the dynamic light scattering (DLS) technique. One milligram per milliliter of samples were measured by DLS, and it was repeated three times. A transmission electron microscope (TEM) was applied to assess the morphologies of samples (0.5 mg/mL) that were prestained with phosphotungstic acid (3%). Native ADI, P-n

(ADI), PP-n(ADI), and PP-n(ADI)/glucose (1 mg/mL, by ADI mass) were labeled with FITC and analyzed *via* agarose gel electrophoresis. The molar ratio of FITC to samples was 5. Gel running electrophoresis was conducted for 30 min on agarose gel (1%). One milligram per milliliter of samples were lyophilized, and they were measured by the Fourier transform infrared spectroscopy (FT-IR) analysis. The UV–visible absorption of sample solutions (0.5 mg/mL) was measured using a spectrophotometer.

To test the surface hydrophobicity of samples, the static water contact angles of samples were measured. Briefly, 1 mg/mL of samples were added onto the surface of a silicon slice, and N_2 was used to dry the surface solution forming a film. Then, we added a drop of water onto the film and recorded the static water contact angle.

2.3 The test of samples' specific activities

The specific activities of samples were measured by an ELISA kit. About 0.1 mg/mL of samples were coincubated with Arg (50 mM) at 37°C, and the process lasted 10 min. Then, an Arg assay kit was applied to quantify the residual Arg, and the enzymatic activity was determined according to the definition. The specific activity was defined as the formula: specific activity (IU/mg) = Enzyme activity/Enzyme concentration.

Then, the specific activities of native ADI and PP-n(ADI), which were preincubated with the same volume of fresh mice serum at 37°C, were tested every 10 days, and it was continued for 60 days. Furthermore, to verify the protective effects of nanogels on therapeutic enzymes, native ADI and PP-n(ADI) were incubated with or without protease (trypsin, 2.0 μM) at 37°C for a day, and their enzymatic activities were also tested. In addition, the specific activities of native ADI and PP-n(ADI), which were stored at different temperatures or in solutions with different pH values, were also tested.

2.4 The glucose responsiveness of samples

To test the glucose-responsive activity of samples, a certain amount of native ADI and PP-n(ADI) was incubated with Arg solution (100 mM) at 37°C, and the concentrations of residual Arg were measured by an Arg assay kit every 1 min. The process lasted for 10 min. Furthermore, the enzyme activities of PP-n(ADI) that was incubated with glucose solution (1, 6, and 10 mM) and an equal volume of serum were also tested according to the above-mentioned methods.

2.5 The cytotoxicity of nanogels

Human umbilical vein endothelial cells (HUVECs) were used to test the cytotoxicity by a CCK-8. Cells were inoculated into a 96-well plate and cultured in a cell incubator for 24 h. Then, fresh medium that contained different concentrations of PP-n(BSA) was employed to replace the culture medium, and untreated cells were used as the control. Each group had six replicates. After 48 h of culture, we added CCK-8 solution to each well, and the absorbance at 450 nm of each well was measured. The cell viability (%) = [absorbance (test well)$_{450\,nm}$ − absorbance (blank well)$_{450\,nm}$]/[absorbance (control well)$_{450\,nm}$ − absorbance (blank well)$_{450\,nm}$] × 100 [30].

2.6 Cell viability assay

Michigan Cancer Foundation-7 (MCF-7) cells were used as target cells to evaluate the cell suppression effects of samples by using a CCK-8. MCF-7 cells (5,000 cells per well) were inoculated into a 96-well plate and cultured in a cell incubator for 24 h. Then, the medium was replaced with a fresh one that contained different concentrations of samples. At 48 h, we added CCK-8 solution into each well, and the cell viability was assessed. Cells without the treatment of samples were used as the control, and the cell viability (%) = [absorbance (test well)$_{450\,nm}$ − absorbance (blank well)$_{450\,nm}$]/[absorbance (control well)$_{450\,nm}$ − absorbance (blank well)$_{450\,nm}$] × 100 [30]. Furthermore, the apoptosis of MCF-7 cells induced by samples was measured by using AnnexinV-FITC/PI double staining.

2.7 The intracellular activity of PP-n(ADI)

The ratio of Cit to Arg in cells that were treated with samples was tested. Briefly, MCF-7 cells were inoculated into a six-well plate and cultured in a cell incubator for 24 h. Then, different concentrations of samples were used to treat cells. The treated cells were washed and detached

with trypsin after 24 h. We further added distilled water to disperse the cells, and the cells were vortexed and centrifuged for 30 min at 12,000 rpm. Finally, we collected the resulting supernatant and used the corresponding assay kits to quantify the Arg and Cit in cells.

2.8 The blood circulation of samples

Similar to what we did before [31], we randomly divided healthy Kunming mice into two groups, and each group had six mice. FITC-labeled native ADI and PP-n(ADI) (~1 mg by ADI mass) were intravenously single-dose injected into the corresponding mice. After the injection, we collected the mice blood at selected time points and obtained mice plasma by gentle centrifugation. Finally, a microplate reader was used to measure the fluorescence intensity of the dilute plasma.

2.9 The *in vivo* activity of PP-n(ADI)

We randomly divided healthy Kunming mice into two groups, and each group had six mice. Samples (~1 mg by ADI mass) were intravenously injected into the corresponding mice once. After the injection, we cut the mice tail to collect mice blood at certain time points and centrifuged the blood to obtain mice plasma. The Cit and Arg in fresh mice plasma were quantified by the assay kits.

2.10 The biological safety of samples

We randomly divided healthy Kunming mice into two groups, and each group had six mice. According to our previous study, samples (~1 mg by ADI mass) were intravenously injected into the corresponding mice once [32]. One week after injection, we euthanized the mice and obtained their main organs, which were further stored overnight in paraformaldehyde solution (4%). Then, organs were carefully washed twice with buffer solution and embedded in paraffin. Finally, we section the embedded organs and stained the tissue sections with hematoxylin–eosin (H&E), and the resulting H&E staining tissue sections were observed under a microscope.

2.11 Statistical analysis

Statistical comparisons were achieved using GraphPad Prism 7.04 software. Results are presented as mean ± SEM.

3 Results and discussion

The morphology and diameter of prepared nanogels were characterized as shown in Figure 1. The diameter of P-n(ADI) (16.58 ± 5.18 nm) was significantly larger than that of native ADI (6.04 ± 1.34 nm), implying the formation of poly(APBA) shell on the ADI surface, but it should be noted that not all ADI was encapsulated into P-n(ADI), and the loading efficiency was 87.67 ± 5.29%. The coupling of PEG to P-n(ADI) further increased in size to 22.58 ± 7.68 nm. Furthermore, the diameter of PP-n(ADI)/glucose was 23.20 ± 6.70 nm, which was nearly not different from that of PP-n(ADI). Theoretically, the formation of polymeric shells on ADI and the further coupling of PEG could gradually increase the size of nanoparticles. Therefore, the size changes implied that the preparation process met our design expectations. PP-n(ADI) potentially improved the *in vivo* application efficiency of ADI because nanogels avoided the removal of ADI by the kidney, which often metabolically cleared drugs smaller than 10 nm [33]. The representative TEM image of samples (the inset picture in Figure 1) presented that they were both spherical shapes and had homogeneous dispersion implying the protection of nanogels to ADI. It had been proved that nanomedicines possessed optimal *in vivo* performances including long blood circulation time, low immunogenicity, and excellent targeting ability should be with the appropriate size (10–100 nm) and regular structure [34]. Therefore, the above results demonstrated that nanogels could potentially be used as excellent delivery vectors for ADI.

As shown in the agarose gel electrophoresis analysis (Figure 2a), FITC-labeled native ADI moved toward positive electrodes because of its electronegativity (Figure 2b). After encapsulation, the zeta potentials of P-n(ADI) and PP-n(ADI) became positive, and therefore, they both moved toward negative electrodes. The high zeta potential of polymeric nanoparticles could result in their rapid *in vivo* clearance. For example, it had been reported that micelles (25 ± 6 nm) with a zeta potential of 37.0 ± 2.9 mV were mostly accumulated in liver tissues [35]. On the

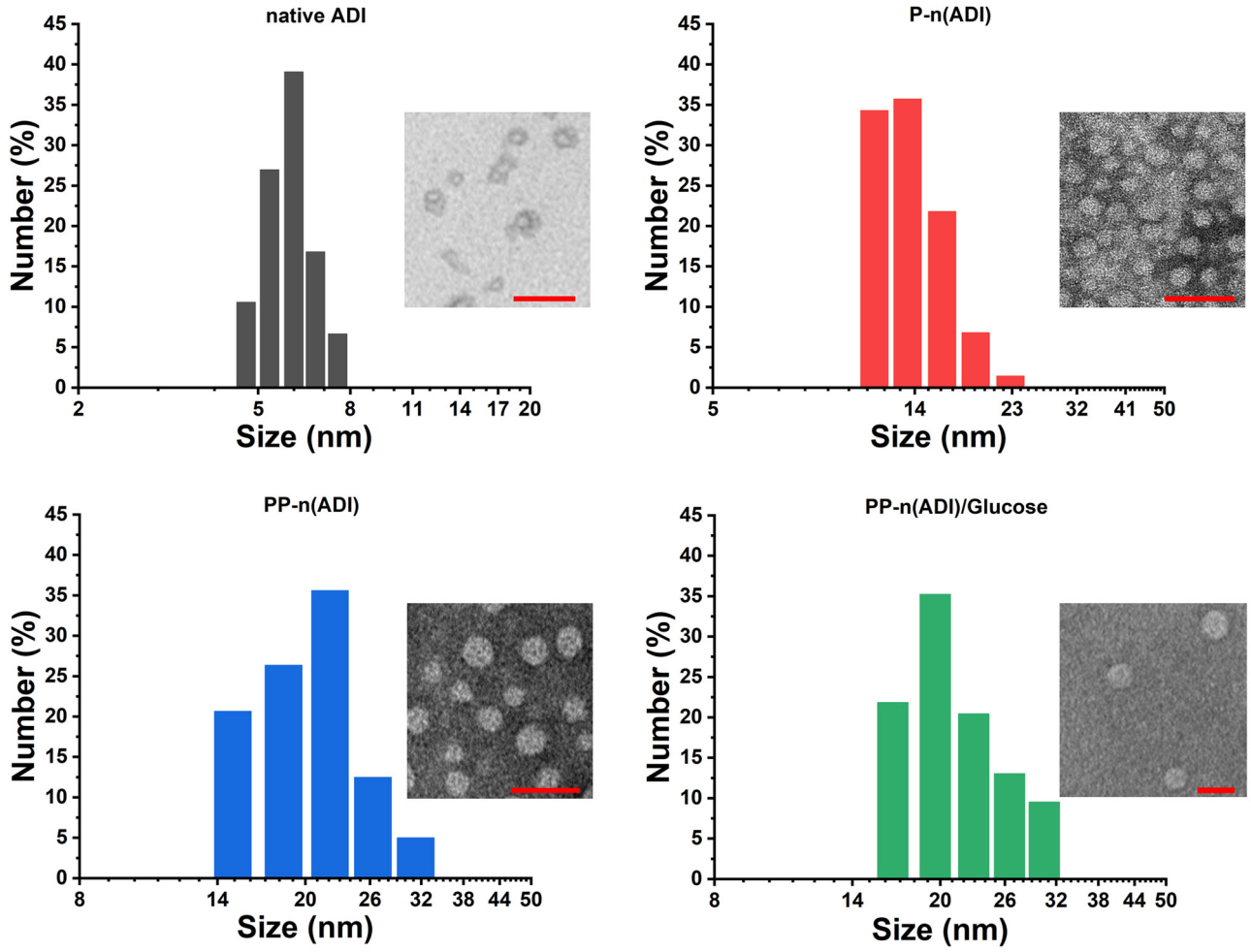

Figure 1: The size distribution of samples. The inset pictures were the corresponding TEM images. The scale bar was 50 nm.

contrary, the accumulation of micelles (27 ± 6 nm) with a zeta potential of 3.6 ± 0.8 mV in liver tissues was much lower. Therefore, although the surface potential of PP-n (ADI) was slightly positive (2.3 ± 1.1 mV), it would not result in the nonspecific clearance of PP-n(ADI) in animals. The surface components and structure of samples were further characterized. For P-n(ADI), the appearance of new peaks (1426.74, 1335.10, and 709.85 cm^{-1}) in the FT-IR spectrum was attributed to the phenylboronic acid (Figure 2c) [36], indicating the successful formation of poly(APBA) shell on the surface of ADI. New peaks at 2881.62, 1103.03, 959.46, and 846.36 cm^{-1} were shown in the spectrum of PP-n(ADI), indicating the successful coupling of PEG to P-n(ADI) [37]. Glucose can be bound to PP-n(ADI) since the spectrum exhibited the typical peaks of glucose at 1427.63 cm^{-1}. The binding of glucose to PP-n(ADI) could potentially prolong its circulation time since the autologous glucose was not perceived as a foreign material by the immune system. Furthermore, the autologous glucose may endow PP-n(ADI) with the ability to target lesions due to the associated diseases consuming a lot of glucose. As an example, glucose could be conjugated to nanomedicines realizing the specific targeting and subsequent treatment of cancers [38]. UV-visible spectrum further proved that the polymeric shells could efficiently shield ADI. Native ADI as a kind of protein showed the characteristic peak at 280 nm. On the contrary, the formation of a polymeric shell on ADI shielded this characteristic peak (Figure 2d).

The water contact angle of the films that were respectively formed by native ADI, P-n(ADI), PP-n(ADI), and PP-n(ADI)/Glucose was measured. As shown in Figure 3, the water contact angle of the film formed by P-n(ADI) was 40.0 ± 3.1°, while that of the film formed by native ADI was 35.5 ± 2.4°, indicating that the poly(APBA) shell increased the hydrophobicity of the system. At physiological pH, the uncharged phenylboronic acid was hydrophobic because of the existence of the benzene ring,

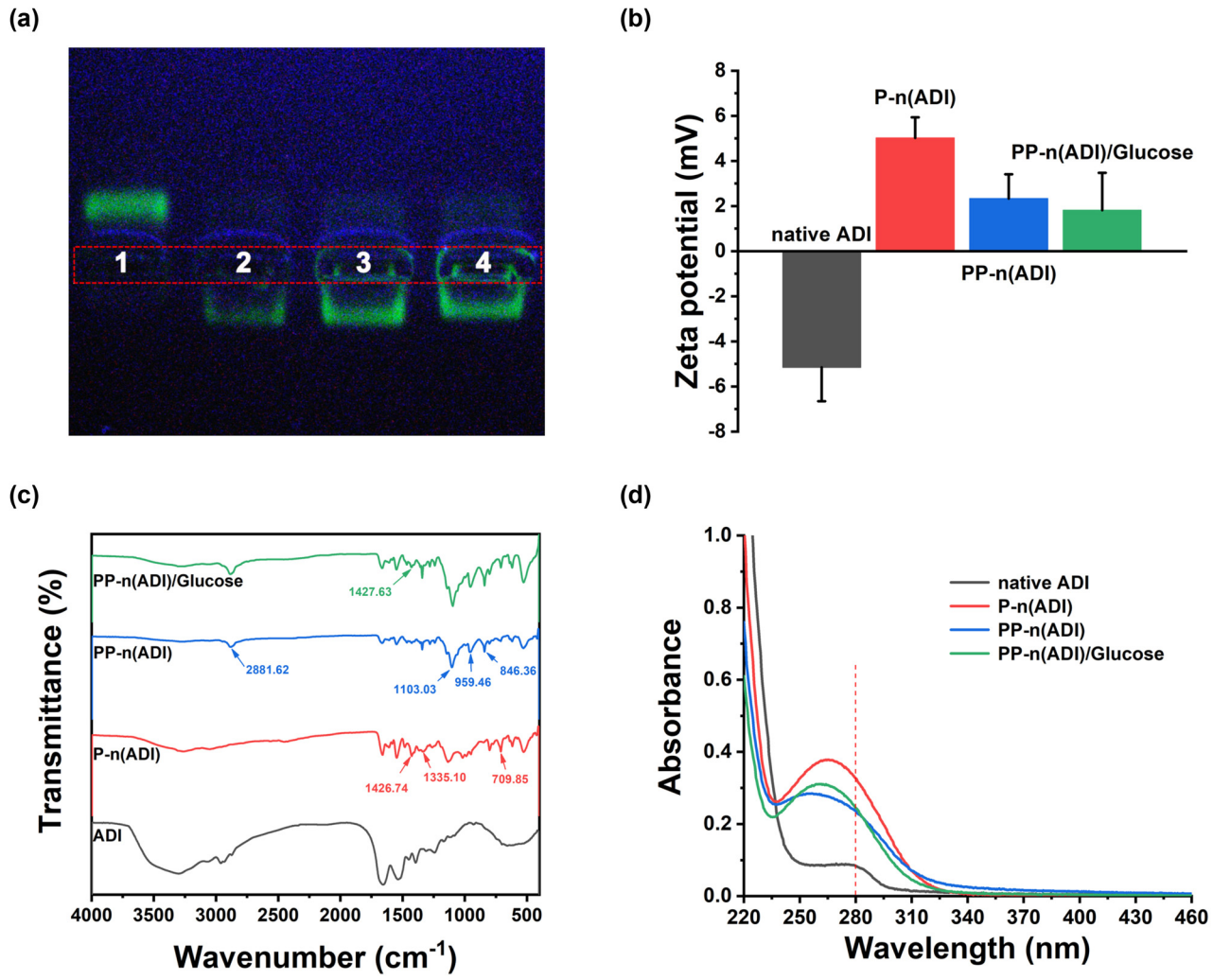

Figure 2: (a) Native ADI (1), P-n(ADI) (2), PP-n(ADI) (3), and PP-n(ADI)/Glucose (4) were analyzed by agarose gel electrophoresis. (b) Zeta potential of corresponding samples. (c) FT-IR spectra of corresponding samples. (d) The UV-visible spectrum of corresponding samples.

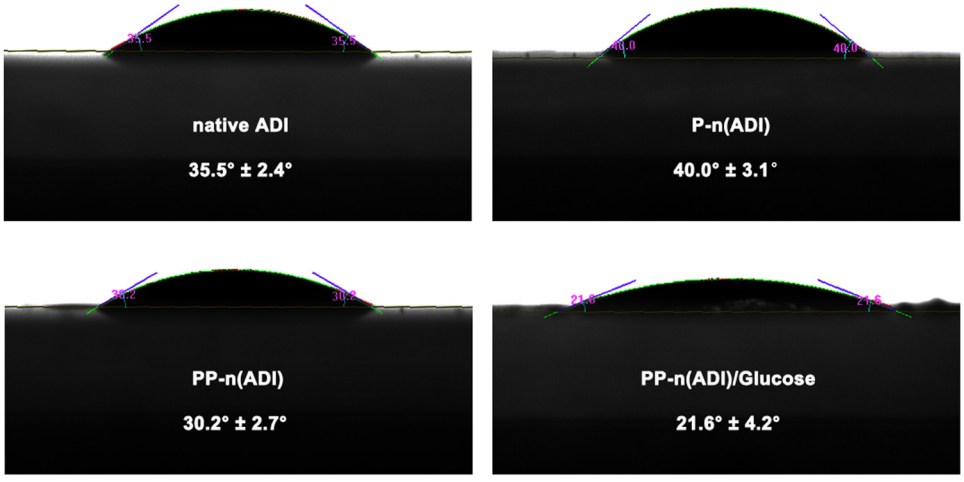

Figure 3: The films were respectively formed by corresponding samples, and their water contact angle was measured.

resulting in the hydrophobicity of the polymer layer on the surface of ADI. When phenylboronic acid could react with glucose to form hydrophilic phenylborates, the hydrophobic polymer layer turned hydrophilic. Furthermore, the coupling of PEG and the binding of glucose improved the hydrophilicity of the system. The hydrophilicity of PP-n(ADI)/Glucose could reduce the protein adsorption and the capture of immune cells, potentially prolonging its circulation time [39]. Taken together, these results indicated that the developed nanogels could successfully encapsulate ADI, and the resulting PP-n(ADI) showed excellent physicochemical properties, facilitating its *in vivo* application.

To investigate the effect of the preparation process on therapeutic enzymes, the activity maintenance of ADI was tested. The specific activity of PP-n(ADI)/Glucose was similar to native ADI's specific activity (Figure 4a), demonstrating that the preparation process would not result in the inactivation of ADI. Therefore, taking advantage of physical interaction to encapsulate therapeutic enzymes was a more suitable method compared with chemical PEGylation and immobilization, which could result in the inactivation of therapeutic enzymes. To further demonstrate the glucose responsiveness of PP-n(ADI), the degradation efficiency of Arg was tested. As shown in Figure 4b, PP-n(ADI) had a low degradation efficiency of Arg, but its efficiency was rapidly improved after incubation with glucose or serum. Importantly, the activity of serum-incubated PP-n(ADI) was similar to that of native ADI, indicating the efficient *in vivo* catalytic activity of PP-n(ADI). These results demonstrated that the encapsulation of therapeutic enzymes in nanogels did not cause damage to them.

In addition, the results indicated that the binding of glucose to nanogels restored the high-efficiency *in vivo* activity of ADI. That is because the binding of glucose could reduce the rigidity of the nanogel shell to endow the internal ADI with more flexibility [28], efficiently increasing the fitness of the ADI active site to Arg. And Arg could readily diffuse through the flexible poly (APBA)/glucose shell, maintaining the degradation efficiency of ADI.

We further tested the influence of nanogels on the stability of ADI. Samples were stored at different temperatures for 30 min. As shown in Figure 5a, nanogels could effectively maintain the thermostability of ADI, while the activity of native ADI was rapidly decreased when the temperature was adjusted to higher than 55°C. Besides, the activities of PP-n(ADI) stored in solutions with different pH values for 30 min were similar, further proving the protective effects of nanogels on therapeutic enzymes (Figure 5b). When samples were pre-incubated with the same volume of fresh mice serum and stored at 37°C, native ADI rapidly lost its activity as the increase of storage time, and it was only ~10% of its initial activity after 30 days of storage (Figure 5c). After 60 days, in contrast, the activity of PP-n(ADI) was still ~60% of its initial activity, implying the protective effects of nanogels on therapeutic enzymes. In addition, the activity maintenance of native ADI and PP-n(ADI), which were

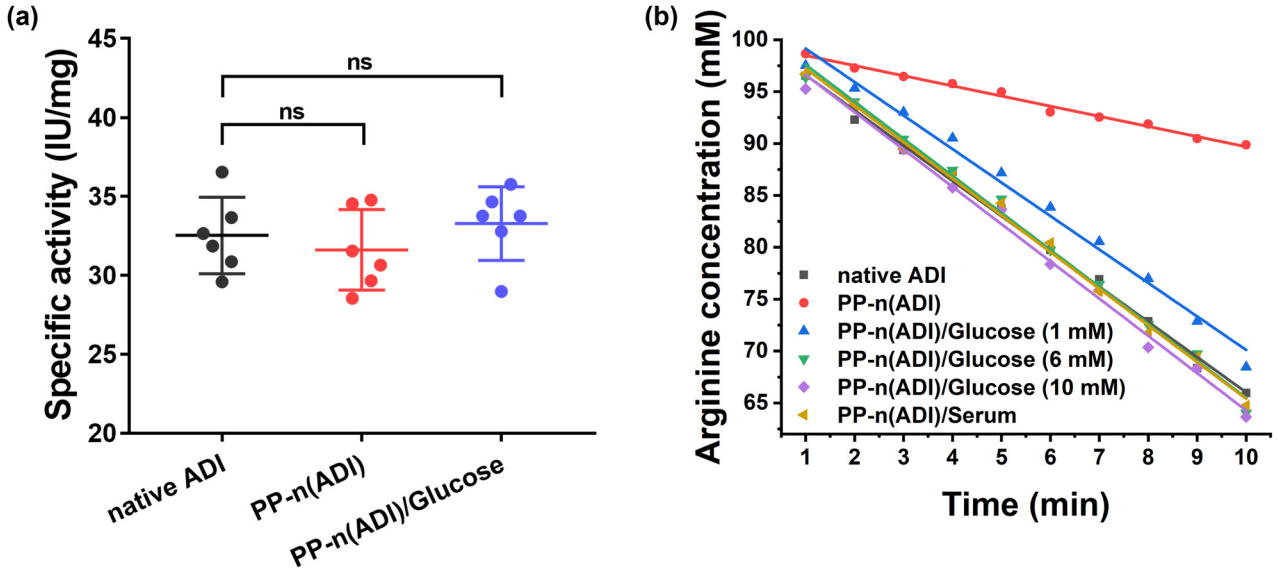

Figure 4: (a) The measurement of the specific activities of samples. The significance level was $^{ns}p > 0.05$. (b) Arg was incubated with different samples and its concentration change in 10 min was measured.

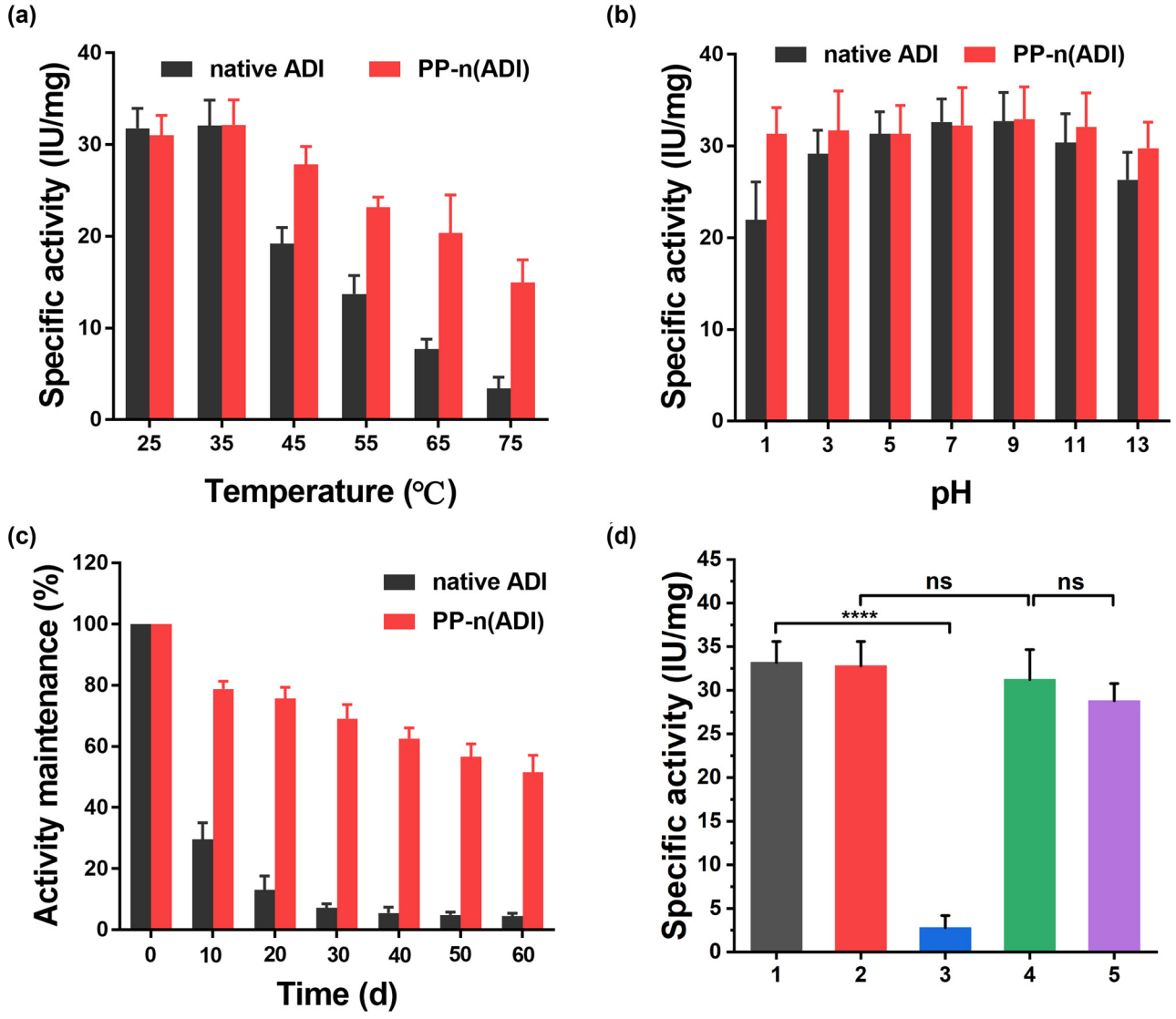

Figure 5: (a) The measurement of the specific activities of samples that were stored at different temperatures for 30 min. (b) The measurement of the specific activities of samples that were stored in solutions with different pH values for 30 min. (c) Samples were pre-incubated with the same volume of fresh mice serum and stored at 37°C for 60 days, and their activity was measured every 10 days. (d) Before and after incubation with trypsin, the specific activity of samples was measured. 1: native ADI; 2: PP-n(ADI); 3: native ADI treated with trypsin; 4: PP-n(ADI) treated with trypsin; 5: PP-n(ADI) first treated with glucose and then treated with trypsin. The significance levels were ****$p < 0.0001$ and $^{ns}p > 0.05$.

both incubated with trypsin, was tested (Figure 5d). The proteases could degrade native ADI and result in its activity loss, while nanogels could efficiently protect ADI from the degradation of proteases. The specific activity of PP-n(ADI) incubated with trypsin was similar to that of native ADI, demonstrating the protective effects of nanogels. Furthermore, to prove whether the nanogel could still resist the attack of proteases when glucose was bound with the nanogel, we first pretreated PP-n(ADI) with glucose and then treated it with trypsin. The activity of the corresponding PP-n(ADI) was still similar to that of native ADI. These results indicated that the rigid nanogels could maintain the *in vitro* stability of ADI by restraining conformational changes in ADI. The stability enhancement of therapeutic enzymes can facilitate their transportation and storage dramatically increasing the possibility of clinical translation.

Figure 6a shows the result of circular dichroism (CD) of the samples. The secondary structure of native ADI treated with trypsin was destroyed. On the contrary, the secondary structure of ADI could be well stabilized by nanogels. These results indicated that nanogels fixed

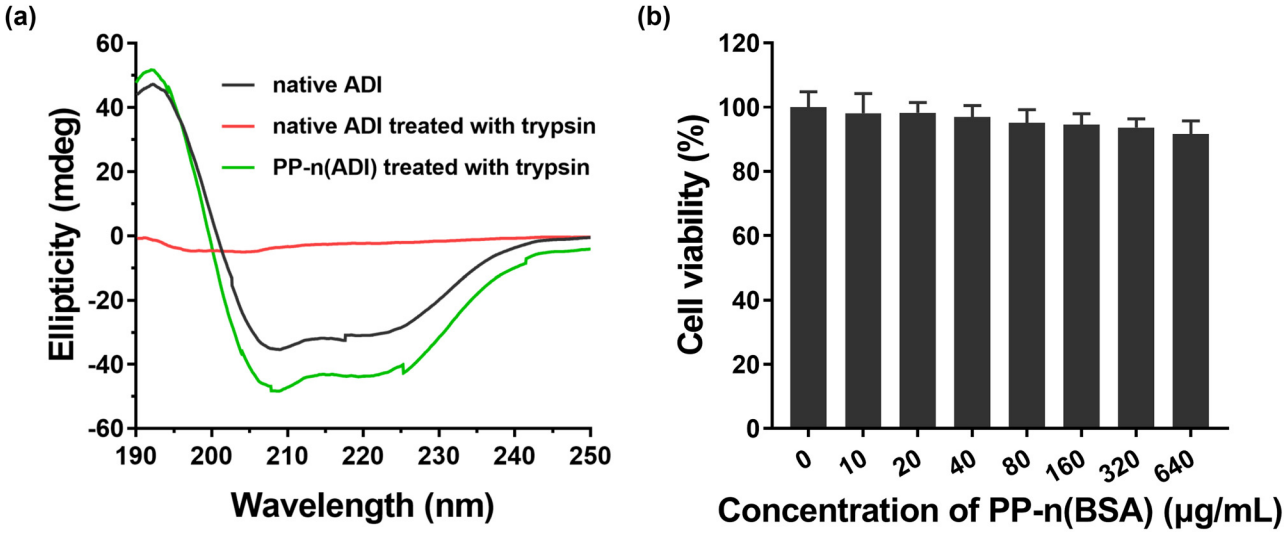

Figure 6: (a) CD analysis of native ADI, native ADI treated with trypsin, and PP-n(ADI) treated with trypsin. (b) Cytotoxicity of different concentrations of PP-n(BSA) in HUVECs.

the structure of therapeutic enzymes leading to the maintenance of their activity. To evaluate the cytotoxic effects of nanogels, BSA was selected as the model protein to prepare PP-n(BSA). That is because BSA had no function and the results would only show the effect of nanogels on cells, avoiding interference from the internal therapeutic enzymes. HUVECs incubated with 640 μg/mL of PP-n(BSA) still maintained as high as 90% viability (Figure 6b), which demonstrated that nanogels as a drug delivery vehicle had suitable cytocompatibility.

MCF-7 cell is a kind of ASS1-deficient tumor cell, and it can be killed by ADI-based Arg deprivation. Here, MCF-7 cells were treated with samples and their cell viabilities were also tested. As shown in Figure 7a, the cell viability was rapidly decreased with the concentration increase of PP-n(ADI). The viability of the PP-n(ADI) (100 ng/mL)-treated MCF-7 cells was ~20% having no difference from that treated with the same concentration of native ADI. It was found that the change of the intracellular amino acid ratio led to cytotoxicity. The MCF-7 cells' intracellular ratio of Cit to Arg was increased with the increase in samples' concentration (Figure 7b). The apoptosis of MCF-7 cells was also measured by AnnexinV-FITC/PI double staining (Figure 7c). Samples could induce the apoptosis of MCF-7 cells, and PP-n(ADI) was potentially more effective because nanogels would alter the cellular interaction of ADI [29]. In conclusion, nanogels had low cytotoxicity and could efficiently maintain the function of therapeutic enzymes.

As depicted in Figure 8a, the blood circulation half-life of PP-n(ADI) was ~12 h, which was much longer than that of native ADI (~2 h). The nanogels significantly prolonged the circulation time of therapeutic enzymes mainly owing to the shielding protection of PEG. Besides, the binding of autologous glucose to the surface of nanogels could avoid the capture of the reticuloendothelial system [40]. The initial ratio of Cit to Arg in mice plasma was 0.56 ± 0.06, and once we intravenously injected the samples, its value was immediately increased to a few hundred (Figure 8b). However, the ratio of Cit to Arg in mice plasma was rapidly decreased in the native ADI group, and it returned to normal after 96 h. In contrast, PP-n(ADI) had a relatively long blood circulation time, and it could realize the sustained degradation of Arg in mice plasma. Even after a week, in the PP-n(ADI) group, the ratio of Cit to Arg in mice plasma was still more than 10. We have given one injection of samples into mice, and their main organs were obtained. We stained histological sections with H&E, and the results showed that samples did not have obvious damage to animals (Figure 8c), indicating the excellent biocompatibility of nanogels. This may be because nanogels did not cause excessive oxidative stress [41]. In addition, Arg deprivation would not damage normal cells because they can convert Cit to Arg via the catalysis of ASS1, indicating the biosafety of ADI based. From the *in vivo* performance of PP-n(ADI), it could be concluded that the encapsulated therapeutic enzymes still possessed efficient *in vivo* activity, and nanogels did not further increase side effects. Therefore, this kind of nanogel was an excellent delivery platform for therapeutic enzymes, and they could serve as novel therapeutic enzyme formulations for various disease treatments, including tumor therapy, antibacterial treatment, and anti-inflammatory therapy [7,42,43].

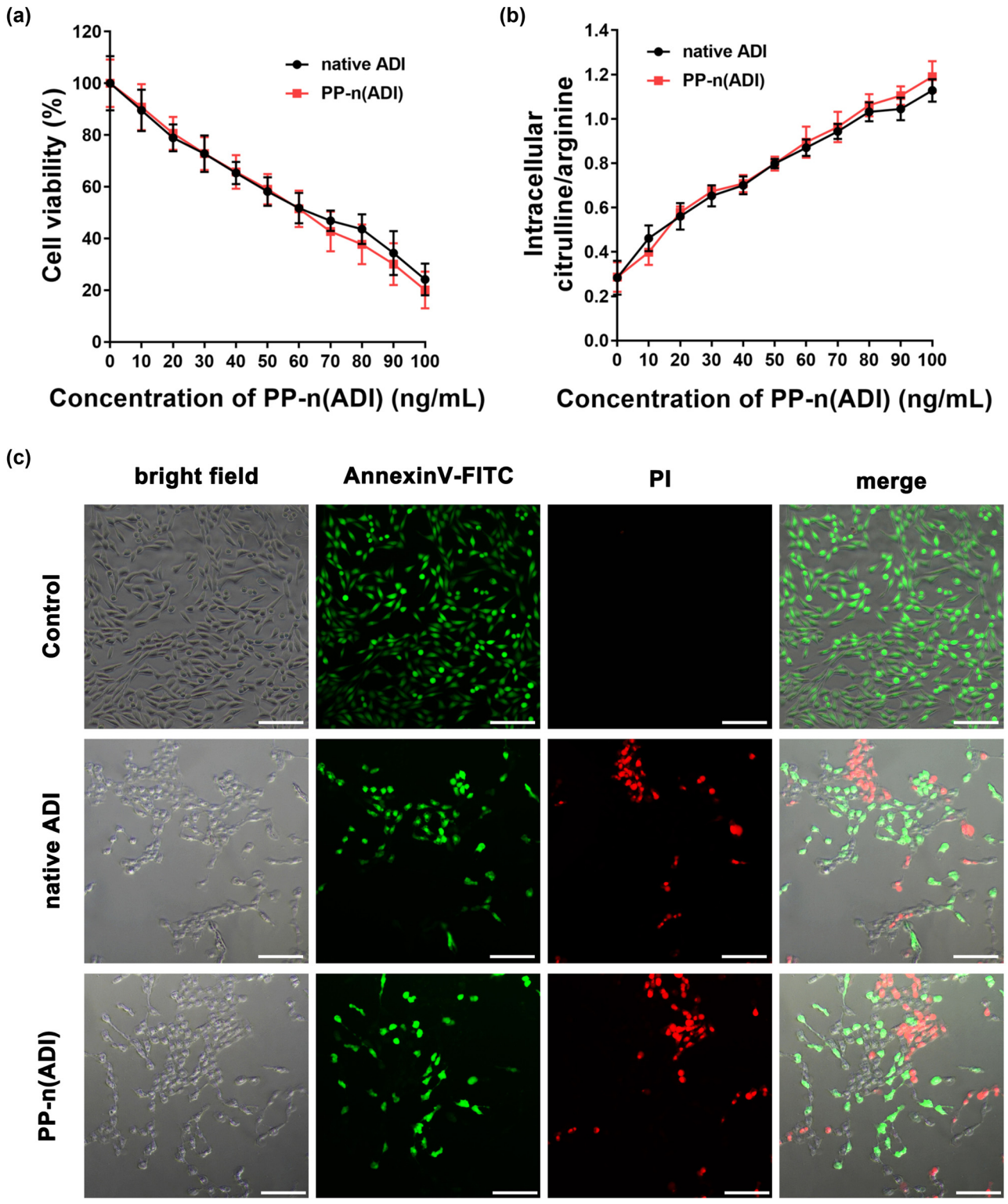

Figure 7: (a) The cell viability of MCF-7 cells that were treated with various concentrations of samples. (b) MCF-7 cells were incubated with various concentrations of samples, and the ratio of Cit to Arg in them was tested. (c) Fluorescence microscopy images showing the apoptosis of MCF-7 cells treated with native ADI and PP-n(ADI) (100 ng/mL) by AnnexinV-FITC/PI double staining. The scale bar is 100 μm.

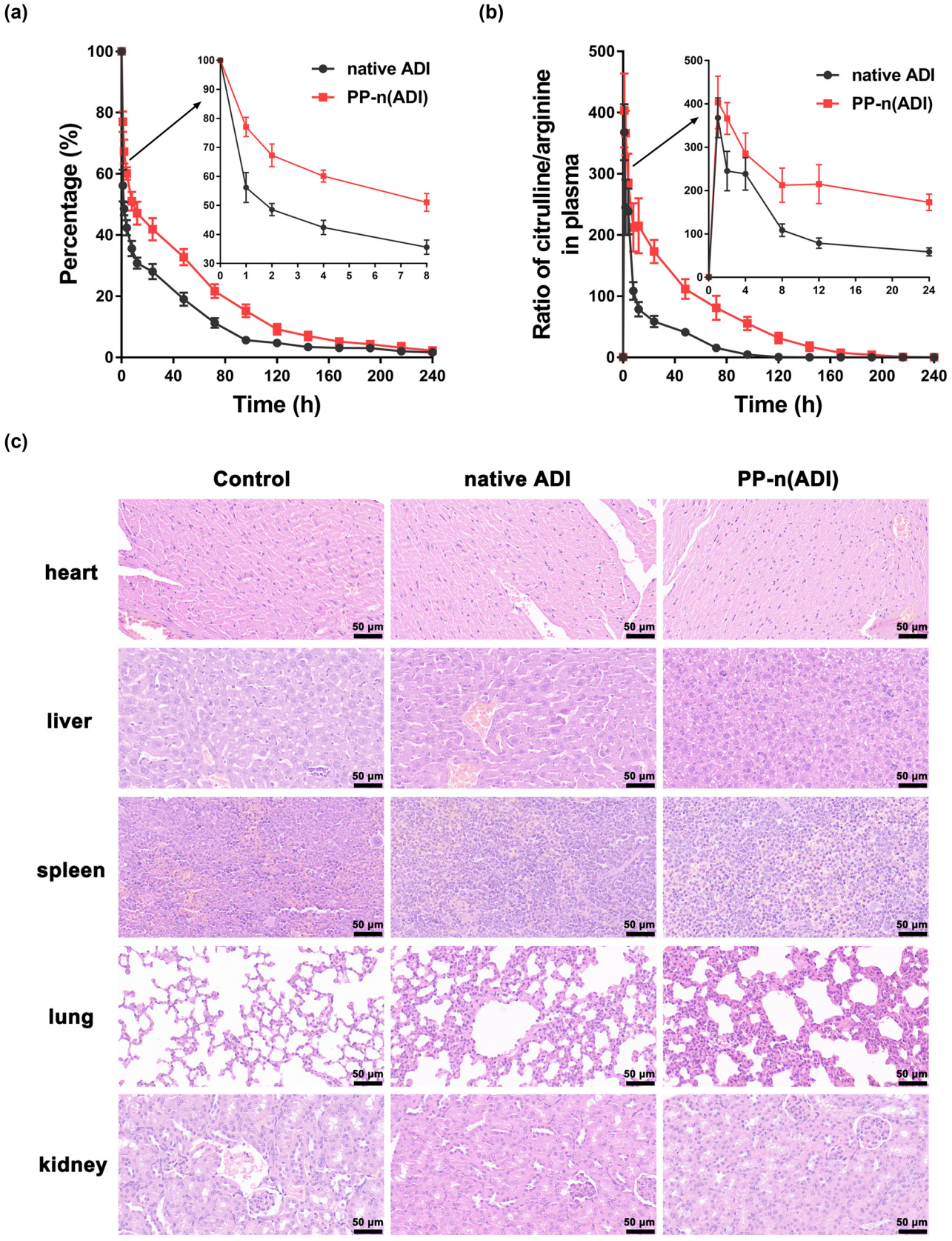

Figure 8: (a) The blood circulation time of samples. FITC was used to label ADI. (b) Samples (~1 mg) were intravenously injected into the mice once, and the ratio of Cit to Arg in corresponding mice plasma was measured. (c) Images of H&E staining of histological sections of organs.

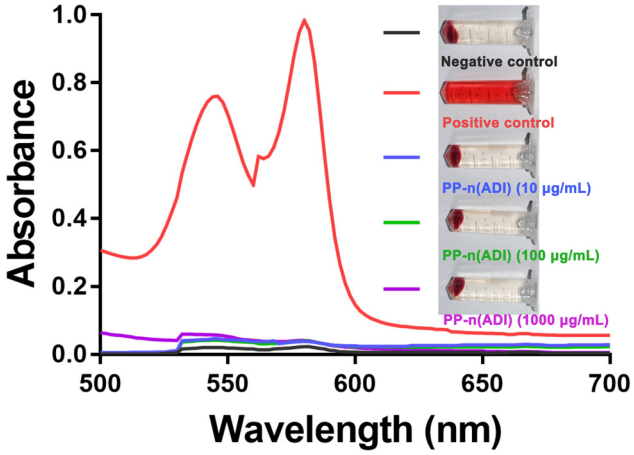

Figure 9: Hemolytic activities of PP-n(ADI) and comparison with saline (negative control) and distilled water (positive control).

To further study the biocompatibility of PP-n(ADI) *in vivo*, hemolytic activity tests were performed to evaluate blood compatibility. No hemolysis was observed in the groups of PP-n(ADI) (Figure 9), which demonstrates that nanogels were biocompatible as a drug delivery vehicle.

4 Conclusions

Glucose-responsive nanogels were synthesized by forming a polymeric shell containing phenylboronic acid groups on a therapeutic enzyme surface. These nanogels could efficiently restrain conformational changes in therapeutic enzymes, dramatically maintaining their *in vitro* stability. When applied *in vivo*, furthermore, phenylboronic acid molecules located at the surface of nanogels could bind with autogenous glucose, leading to the hydrophilicity and flexibility increase in the polymeric shell. Then, substrate molecules are easily diffused through the flexible polymeric shell, effectively maintaining their *in vivo* catalytic activity. Moreover, the flexible polymeric shell can still protect ADI from degradation and improve its *in vivo* stability. This kind of nanogel can significantly improve the *in vitro* stability of therapeutic enzymes and maintain their *in vivo* activity by the flexible change of the nanogel rigidity, facilitating the exploitation of new therapeutic enzyme formulations. In the present study, the researchers mainly focused on the *in vivo* efficiency of the drug. We believe that the efficiency of the drug from *in vitro* preparation and storage to clinical *in vivo* application should be considered comprehensively. And we hope our results can inspire others to design more efficient pharmaceutical preparations.

Funding information: This work was supported by the Nature Science Foundation of Shandong Province (No. ZR2019BC020) and the National Nature Science Foundation of China (No. 52103170).

Author contributions: All authors have accepted responsibility for the entire content of this article and approved its submission.

Conflict of interest: The authors state no conflict of interest.

References

[1] Vellard M. The enzyme as drug: application of enzymes as pharmaceuticals. Curr Opin Biotech. 2003;14:444–50.
[2] De Duve C. The significance of lysosomes in pathology and medicine. Proc Inst Med Chic. 1966;26:73–6.
[3] Wu Q, He Z, Wang X, Zhang Q, Wei Q, Ma S, et al. Cascade enzymes within self-assembled hybrid nanogel mimicked neutrophil lysosomes for singlet oxygen elevated cancer therapy. Nat Commun. 2019;10:1–14.
[4] Qin M, Cao Z, Wen J, Yu Q, Liu C, Wang F, et al. An antioxidant enzyme therapeutic for COVID-19. Adv Mater. 2020;32:2004901.
[5] Meng Y, Sohar I, Sleat DE, Richardson JR, Reuhl KR, Jenkins RB, et al. Effective intravenous therapy for neurodegenerative disease with a therapeutic enzyme and a peptide that mediates delivery to the brain. Mol Ther. 2014;22:547–53.
[6] Puzzo F, Colella P, Biferi MG, Bali D, Paulk NK, Vidal P, et al. Rescue of Pompe disease in mice by AAV-mediated liver delivery of secretable acid α-glucosidase. Sci Transl Med. 2017;9(418):eaam6375.
[7] Li X, Yang Y, Wang Z, Ju H, Fu X, Zou L, et al. Multistage-responsive nanocomplexes attenuate ulcerative colitis by improving the accumulation and distribution of oral nucleic acid drugs in the colon. ACS Appl Mater Inter. 2022;14:2058–70.
[8] Dean SN, Turner KB, Medintz IL, Walper SA. Targeting and delivery of therapeutic enzymes. Ther Deliv. 2017;8:577–95.
[9] Vinogradov VV, Avnir D. Exceptional thermal stability of therapeutical enzymes entrapped in alumina sol-gel matrices. J Mater Chem B. 2014;2:2868–73.
[10] Fuhrmann G, Leroux JC. Improving the stability and activity of oral therapeutic enzymes-Recent advances and perspectives. Pharm Res. 2014;31:1099–105.
[11] Qi H, Yang L, Shan P, Zhu S, Ding H, Xue S, et al. The stability maintenance of protein drugs in organic coatings based on nanogels. Pharmaceutics. 2020;12:115.
[12] Karamitros CS, Yashchenok AM, Möhwald H, Skirtach AG, Konrad M. Preserving catalytic activity and enhancing biochemical stability of the therapeutic enzyme asparaginase by biocompatible multilayered polyelectrolyte microcapsules. Biomacromolecules. 2013;14:4398–406.
[13] Tadepalli S, Yim J, Cao S, Wang Z, Naik RR, Singamaneni S. Metal-organic framework encapsulation for the preservation

and photothermal enhancement of enzyme activity. Small. 2018;14:1702382.
[14] Yari M, Ghoshoon B, Vakili M, Ghasemi B, Y. Therapeutic enzymes: applications and approaches to pharmacological improvement. Curr Pharm Biotechno. 2017;18:531–40.
[15] Veronese FM, Mero A. The impact of PEGylation on biological therapies. BioDrugs. 2008;22:315–29.
[16] Cowan DA, Fernandez-Lafuente R. Enhancing the functional properties of thermophilic enzymes by chemical modification and immobilization. Enzyme Microb Tech. 2011;49:326–46.
[17] Rodriguez-Abetxuko A, Sánchez-deAlcázar D, Muñumer P, Beloqui A. Tunable polymeric scaffolds for enzyme immobilization. Front Bioeng Biotechnol. 2020;8:830.
[18] Bomboi F, Tardani F, Gazzoli D, Bonincontro A, La Mesa C. Lysozyme binds onto functionalized carbon nanotubes. Colloid Surf B. 2013;108:16–22.
[19] Chakraborty S, Joshi P, Shanker V, Ansari Z, Singh SP, Chakrabarti P. Contrasting effect of gold nanoparticles and nanorods with different surface modifications on the structure and activity of bovine serum albumin. Langmuir. 2011;27:7722–31.
[20] Cukalevski R, Lundqvist M, Oslakovic C, Dahlbäck Br, Linse S, Cedervall T. Structural changes in apolipoproteins bound to nanoparticles. Langmuir. 2011;27:14360–9.
[21] Huang R, Carney RP, Stellacci F, Lau BL. Protein-nanoparticle interactions: the effects of surface compositional and structural heterogeneity are scale dependent. Nanoscale. 2013;5:6928–35.
[22] Kao KC, Lin TS, Mou CY. Enhanced activity and stability of lysozyme by immobilization in the matching nanochannels of mesoporous silica nanoparticles. J Phys Chem C. 2014;118:6734–43.
[23] Zhang P, Sun F, Tsao C, Liu S, Jain P, Sinclair A, et al. Zwitterionic gel encapsulation promotes protein stability, enhances pharmacokinetics, and reduces immunogenicity. P Natl Acad SCI USA. 2015;112:12046–51.
[24] Kim SH, Kim KR, Ahn DR, Lee JE, Yang EG, Kim SY. Reversible regulation of enzyme activity by pH-responsive encapsulation in DNA nanocages. ACS Nano. 2017;11:9352–9.
[25] Chapman R, Stenzel MH. All wrapped up: Stabilization of enzymes within single enzyme nanoparticles. J Am Chem Soc. 2019;141:2754–69.
[26] Johnson KA. Role of induced fit in enzyme specificity: a molecular forward/reverse switch. J Biol Chem. 2008;283:26297–301.
[27] Chen C, Gu Y, Deng L, Han S, Sun X, Chen Y, et al. Tuning gelation kinetics and mechanical rigidity of β-hairpin peptide hydrogels via hydrophobic amino acid substitutions. ACS Appl Mater Inter. 2014;6:14360–8.
[28] Wang Q, Wang H, Chen Q, Guan Y, Zhang Y. Glucose-triggered micellization of Poly (ethylene glycol)-b-poly (N-isopropylacrylamide-co-2-(acrylamido) phenylboronic acid) block copolymer. ACS Appl Polym Mater. 2020;2:3966–76.
[29] Qi H, Wang Y, Yuan X, Li P, Yang L. Selective extracellular arginine deprivation by a single injection of cellular non-uptake arginine deiminase nanocapsules for sustained tumor inhibition. Nanoscale. 2020;12:24030–43.
[30] Yang L, Han D, Zhan Q, Li X, Shan P, Hu Y, et al. Blood TfR + exosomes separated by a pH-responsive method deliver chemotherapeutics for tumor therapy. Theranostics. 2019;9:7680.
[31] Qi H, Yang L, Li X, Sun X, Zhao J, Hou X, et al. Systemic administration of enzyme-responsive growth factor nanocapsules for promoting bone repair. Biomater Sci. 2019;7:1675–85.
[32] Qi H, Liu C, Long L, Ren Y, Zhang S, Chang X, et al. Blood exosomes endowed with magnetic and targeting properties for cancer therapy. ACS Nano. 2016;10:3323–33.
[33] Tang L, Yang X, Yin Q, Cai K, Wang H, Chaudhury I, et al. Investigating the optimal size of anticancer nanomedicine. P Natl Acad SCI USA. 2014;111:15344–9.
[34] Blanco E, Shen H, Ferrari M. Principles of nanoparticle design for overcoming biological barriers to drug delivery. Nat Biotechnol. 2015;33:941.
[35] Xiao K, Li Y, Luo J, Lee JS, Xiao W, Gonik AM, et al. The effect of surface charge on in vivo biodistribution of PEG-oligocholic acid based micellar nanoparticles. Biomaterials. 2011;32:3435–46.
[36] Basiruddin S, Swain SK. Phenylboronic acid functionalized reduced graphene oxide based fluorescence nano sensor for glucose sensing. Mat Sci Eng C. 2016;58:103–9.
[37] Elmarzugi NA, Adali T, Bentaleb AM, Keleb EI, Mohamed AT, Hamza AM. Spectroscopic characterization of PEG-DNA biocomplexes by FTIR. J Appl Pharm Sci. 2014;4:6.
[38] Calvaresi EC, Hergenrother PJ. Glucose conjugation for the specific targeting and treatment of cancer. Chem Sci. 2013;4:2319–33.
[39] Simon J, Wolf T, Klein K, Landfester K, Wurm FR, Mailänder V. Hydrophilicity regulates the stealth properties of polyphosphoester-coated nanocarriers. Angew Chem Int Ed. 2018;57:5548–53.
[40] Cvjetinović Đ, Prijović Ž, Janković D, Radović M, Mirković M, Milanović Z, et al. Bioevaluation of glucose-modified liposomes as a potential drug delivery system for cancer treatment using 177-Lu radiotracking. J Control Rel. 2021;332:301–11.
[41] Qi H, Wang Y, Fa S, Yuan C, Yang L. Extracellular vesicles as natural delivery carriers regulate oxidative stress under pathological conditions. Front Bioeng Biotechnol. 2021;810.
[42] Qi H, Shan P, Wang Y, Li P, Wang K, Yang L. Nanomedicines for the efficient treatment of intracellular bacteria: the “ART” principle. Front Chem. 2021;924.
[43] Shan P, Yang F, Qi H, Hu Y, Zhu S, Sun Z. Alteration of MDM2 by the small molecule YF438 exerts antitumor effects in triple-negative breast cancer. Cancer Res. 2021;81:4027–40.